2007

Aerosol Properties Computed from Aircraft-Based Observations during the ACE-Asia Campaign: 1. Aerosol Size Distributions Retrieved from Optical Thickness Measurements

M. Kuzmanoski
University of New South Wales, Sydney, Australia, mkuzm@phys.unsw.edu.au

M. A. Box
University of New South Wales, Sydney, Australia

G. P. Box
University of New South Wales, Sydney, Australia

B. Schmid
Bay Area Environmental Research Institute, Sonoma, California, USA

J. Wang
Brookhaven National Laboratory, Upton, New York, USA

See next page for additional authors

Aerosol Science and Technology, 41:202–216, 2007

ISSN: 0278-6826 print / 1521-7388 online
DOI: 10.1080/02786820601126789

Aerosol Properties Computed from Aircraft-Based Observations during the ACE-Asia Campaign: 1. Aerosol Size Distributions Retrieved from Optical Thickness Measurements

M. Kuzmanoski,[1,2] M. A. Box,[1] G. P. Box,[1] B. Schmid,[2,3] J. Wang,[4] P. B. Russell,[5] H. H. Jonsson,[6] and J. H. Seinfeld[7]

[1]*School of Physics, University of New South Wales, Sydney, Australia*
[2]*Bay Area Environmental Research Institute, Sonoma, California, USA*
[3]*Now at Pacific Northwest National Laboratory, Richland, Washington, USA*
[4]*Brookhaven National Laboratory, Upton, New York, USA*
[5]*NASA Ames Research Center, Moffett Field, California, USA*
[6]*Center for Interdisciplinary Remotely-Piloted Aircraft Studies, Marina, California, USA*
[7]*Department of Chemical Engineering, California Institute of Technology, Pasadena, California, USA*

In this article, aerosol size distributions retrieved from aerosol layer optical thickness spectra, derived from the 14-channel NASA Ames Airborne Tracking Sunphotometer (AATS-14) measurements during the ACE-Asia campaign, are presented. Focusing on distinct aerosol layers (with different particle characteristics) observed in four vertical profiles, we compare the results of two different retrieval methods: constrained linear inversion and a nonlinear least squares method. While the former does not use any assumption about the analytical form of the size distribution, the latter was used to retrieve parameters of a bimodal lognormal size distribution. Furthermore, comparison of the retrieved size distributions with those measured in-situ, aboard the same aircraft on which the sunphotometer was flown, was carried out. Results of the two retrieval methods showed good agreement in the radius ranges from $\sim$0.1 μm to $\sim$1.2–2.0 μm, close to the range of retrievable size distributions from the AATS-14 measurements. In this radius interval, shapes of retrieved and measured size distributions were similar, in accord with close wavelength dependencies of the corresponding optical thicknesses. Additionally, the effect of a size-resolved refractive index on the retrieved size spectra was investigated in selected cases. Retrieval using a constant refractive index pertaining to particle sizes within the range of retrievable size distributions resulted in a size distribution very close to the one retrieved using a size-resolved refractive index.

Received 21 November 2005; accepted 17 November 2006.

This work was carried out while one author (M. K.) was supported by an International Postgraduate Research Scholarship, funded by the Australian Department of Education, Science and Training (DEST). The authors wish to thank the anonymous reviewer for very useful comments and suggestions.

Address correspondence to M. Kuzmanoski, School of Physics, University of New South Wales, Sydney, NSW 2052, Australia. E-mail: mkuzm@phys.unsw.edu.au

1. INTRODUCTION

Aerosol size distribution is, along with particle refractive index and shape, one of important parameters determining their optical properties, such as optical thickness, asymmetry parameter and single scattering albedo. It is highly variable in space and time due to the variability of sources (d'Almeida et al. 1991) and short lifetimes of aerosols. Furthermore, evolution of aerosol sizes by chemical and dynamic processes, such as condensation, coagulation, gas-to-particle conversion (Reid et al. 1998), and particle growth due to water uptake at high relative humidity (Svenningsson et al. 1992) contribute to their variability, and consequently, to variability of the aerosol optical properties.

While aerosol size distributions can be measured in-situ, in different size ranges, using a variety of instruments (McMurry 2000), they can also be derived from measured aerosol optical properties, such as the wavelength dependence of aerosol optical depth (King et al. 1978), or backscattering (Ben-David et al. 1988), or a combination of radiances scattered at different angles and optical depth spectra (Nakajima et al. 1996; Dubovik et al. 1995). These approaches yield integrated size distribution in a vertical column of an atmospheric layer. As no interaction with particles is involved, retrieval of aerosol size distributions from their optical properties has the advantage of giving information on size distributions in ambient conditions. The retrieved size distributions can be used to calculate the column integrated aerosol optical properties, needed as an input into radiative transfer codes (Russell et al. 1999).

During the ACE-Asia campaign, conducted in spring 2001 in Eastern Asia and Northwestern Pacific, a variety of airborne, shipborne and ground-based instruments operated, providing an

extensive set of data [special issue *J. Geophys. Res. Vol.* 108, No. 23, 2003]. Wang et al. (2002) compared the extinction spectra that follow from the aerosol size distributions measured in-situ aboard the CIRPAS (Bluth et al. 1996; Bane et al. 2004) Twin Otter aircraft with those derived from AATS-14 sunphotometer measurements aboard the same aircraft. They found that in the boundary and pollution layers, as well as in the free-tropospheric layers without a significant amount of dust, discrepancies were within the estimated errors. In the dust layers, closure was not achieved, which was attributed to the nonsphericity of dust particles (and interpretation of the measurements of the Aerodynamic Particle Sizer associated with it) as well as horizontal inhomogeneity of these layers. Conversely, information about aerosol size distributions can be inverted from the measured extinction, and size distribution closure can be investigated by comparing to the measured size distribution. Such an aerosol size distribution closure study was performed for the earlier, ACE-2 campaign (Schmid et al. 2000).

In this article, aerosol size distributions retrieved from measured optical thicknesses of distinct layers sampled during the ACE-Asia campaign are presented. Due to non-uniqueness of results of retrieval, two different retrieval methods were used for this purpose, and the corresponding results were inter-compared. The focus was on the same layers studied by Wang et al. (2002) for radiative closure, and comparison of results of the retrievals with in-situ measured size distributions was carried out. Results of calculation of aerosol optical properties from the retrieved size distributions, carried out for one of the vertical profiles studied here, are presented in a separate paper (Part II) (Kuzmanoski et al. 2006). This article also discusses comparison of optical properties resulting from retrieved and measured size distributions, as well as comparison of the modeled extinction-to-backscatter ratio profiles with that derived by Schmid et al. (2003) from combined airborne sunphotometer and shipborne lidar measurements.

2. MEASUREMENTS

Sunphotometer measurements of aerosol optical depth and in-situ size distribution measurements, used in this work, were performed aboard the Twin Otter aircraft. The optical depth measurements were taken using a 14-channel NASA Ames Airborne Tracking Sunphotometer (AATS-14) (Schmid et al. 2003). It measures the directly transmitted solar beam at 14 discrete wavelengths in the range from 0.354 μm to 1.558 μm. The 0.940 μm channel was used for water vapor column retrieval, while the remaining 13 channels were used to derive aerosol optical depth, after corrections for Rayleigh scattering, gaseous absorption (O_3, NO_2, H_2O, and O_2-O_2) and diffuse light. Details about the cloud screening method, calibration, data analysis, and error estimates are given by Schmid et al. (2003).

In-situ aerosol size distribution measurements were carried out using a combination of two instruments: a Differential Mobility Analyzer (DMA) System was used for measurements in the 7.5–500 nm particle radius range, while the 0.25–5 μm radius range was covered by an Aerodynamic Particle Sizer (APS) (Wang et al. 2002). Two DMA systems were used for measurements aboard the Twin Otter aircraft: one of them measured the dry aerosol size distribution, while the other one measured at ambient relative humidity (RH). Wang et al. (2002) describe the measurement procedure, and the method used for integrating these measurements to obtain in-situ measured size distribution in the complete 7.5 nm to 5 μm size range. Hegg et al. (2005) performed tests of the transmission efficiency of the sampling inlet on the CIRPAS Twin Otter aircraft, at an aircraft sampling velocity of 50 m/s. They reported no significant efficiency loss in the particle size range 0.25–1.75 μm, a decrease in efficiency with increasing particle radius to 2.75 μm, and a value slightly greater than 60% at 2.75 μm and larger radii.

3. RETRIEVAL OF AEROSOL SIZE DISTRIBUTIONS FROM OPTICAL THICKNESS MEASUREMENTS

Optical thickness spectra carry information about the aerosol size distribution. Assuming that aerosols are homogeneous spheres, the equation that relates these two aerosol properties is:

$$\tau(\lambda) = \pi \int_{r_a}^{r_b} r^2 Q_{ext}(r, \lambda, m) n(r)\, dr, \qquad [1]$$

where $\tau(\lambda)$ is the aerosol optical thickness, Q_{ext} is Mie extinction efficiency, m is the aerosol refractive index, and $n(r)$ is the aerosol size distribution.

Various methods that have been proposed for solving this equation include those in which an assumption about the analytical form of the size distribution to be retrieved is made (Wang et al. 1989; Yue et al. 1986; Brogniez and Lenoble 1988), as well as methods that make no assumption about the size distribution shape (King et al. 1978; Box et al. 1992; Heintzenberg et al. 1981). In this article, two retrieval methods were used: the constrained linear inversion, and the non-linear least squares methods. A brief overview of the methods is given in the following section.

3.1. Constrained Linear Inversion Method

The constrained linear inversion method for solving the Equation (1) was introduced by Twomey (1977) and developed by King et al. (1978). In this approach (Equation [1]) is discretized, and the size distribution function n(r) is represented by a product of two functions:

$$n(r) = h(r) \cdot f(r), \qquad [2]$$

where $h(r)$ is an assumed, rapidly varying function. Incorporating $h(r)$ into the kernel function, the problem becomes one of finding the slowly varying function, $f(r)$, as a result of the

following linear matrix equation:

$$\tau = \mathbf{A}\mathbf{f} + \varepsilon, \qquad [3]$$

where

$$\tau_j = \tau(\lambda_j), \quad j = 1, 2, \ldots, 13 \qquad [3a]$$

$$A_{ji} = \int_{r_i}^{r_{i+1}} \pi r^2 Q_{ext}(r, \lambda_j, m) h(r)\, dr, \qquad [3b]$$

$$f_i = \bar{f}(r), \quad r_i \le r < r_{i+1}. \qquad [3c]$$

Here, ε is an unknown error vector, due to measurement errors, as well as uncertainties due to the exact form of the kernel function. The problem is solved in a number of iterations. The initial guess of weighting function $h(r)$ is the Junge power law (Junge 1955):

$$h^{(0)}(r) = r^{-(\nu^*+1)}, \qquad [4]$$

where the Junge exponent ν^* is computed from the wavelength dependence of the aerosol optical depth, and the solution is found in the form:

$$f = \left(A^T S_\varepsilon^{-1} A + \gamma H\right)^{-1} A^T S_\varepsilon^{-1} \tau. \qquad [5]$$

Here, S_ε is the measurement covariance matrix, γ is the Lagrange multiplier, and H is the second derivative smoothing matrix (King et al. 1982). Choice of the Lagrange multiplier is discussed by King (1982).

In the next iteration step, the weighting function becomes

$$h^{(1)}(r) = h^{(0)}(r) f(r). \qquad [6]$$

3.2. Non-Linear Least Squares Method

The nonlinear least squares algorithm was used by Wang et al. (1989, 1996) for retrieving aerosol size distributions represented by modified gamma and unimodal and bimodal lognormal functions. They employed the modified Levenberg-Marquardt algorithm (More, 1977), and tested the performance of this method on retrieving size distributions from simulated SAGE II and SAGE III measurements. This algorithm provides a solution, p, of the following constrained least squares problem:

$$\min\{\|F + Jp\| : \|Dp\| \le \Delta\}. \qquad [7]$$

Here, F is a column of residuals given by:

$$F_i(x) = \tau_i - \int_{r_a}^{r_b} \pi r^2 Q_{ext}(r, \lambda_i) n(r; x)\, dr, \qquad [8]$$

where τ_i is the optical thickness measured at the wavelength λ_i, $Q_{ext}(r, \lambda_i)$ is the Mie extinction efficiency, and $n(r; x)$ the aerosol size distribution. x is the set of parameters that defines the aerosol size distribution (function) to be retrieved. The corresponding Jacobian matrix, J, is calculated at x by the use of a forward difference approximation. D is a diagonal scaling matrix, and Δ is the step bound.

The application of the code starts with evaluating the residual column and the Jacobian matrix at the initial estimate of the solution parameters, $x = x_0$. This is followed by calculation of the initial diagonal scaling matrix D_0 and step bound Δ_0 and the Lagrange multiplier ε. The perturbation from the initial solution is estimated as:

$$p = -(J^T J + \varepsilon D^T D)^{-1} J^T F. \qquad [9]$$

In the next iteration step, x is replaced by $x + p$. The procedure is repeated until the desired level of agreement is reached.

3.3. Application of the Size Distribution Retrieval Methods

In this article, the two inversion methods described above were employed to derive aerosol layer size distributions from the aerosol layer optical thicknesses measured using the airborne sunphotometer.

The constrained linear inversion method was applied using the algorithm given by King et al. (1978). The parameters whose values have to be defined prior to the application of the retrieval algorithm are the aerosol refractive index and the upper and lower radii limits. The refractive index is assumed to be constant (not dependent on wavelength or particle size). The sensitivity of the retrieval results to this assumption is investigated later (in Section 4.1.), using size-resolved refractive indices derived by Wang et al. (2002), based on measured chemical composition. For given input parameter values, the result of the inversion is not unique; it depends on the initial estimate of the solution and the number of iterations in the retrieval. Contributions of particles of different sizes to the inverted optical thickness were examined for all retrieved size distributions, to ensure that for the given radii limits all particle sizes with significant contribution to the inverted property were taken into account.

The nonlinear least squares algorithm was implemented by the use of a modified Levenberg-Marquardt algorithm (More 1977) from the SLATEC mathematical library, coupled with a standard Mie code. The Mie code developed by M. Mishchenko (Mishchenko et al. 1999; De Rooij and Van Der Stap 1984), and obtained from www.giss.nasa.gov/∼crmim, was used.

This retrieval algorithm was used to derive the parameters of the bimodal lognormal size distribution:

$$n(r) = \sum_{i=1}^{2} \frac{N_{0i}}{\sqrt{2\pi}\sigma_i} \exp\left(-\frac{(\ln r - \ln r_{mi})^2}{2\sigma_i^2}\right). \qquad [10]$$

Each mode is defined with three parameters: N_{0i} is the total particle concentration, and r_{mi} and σ_i are the modal radius and width of the i*th* mode. Although three modes (nucleation, accumulation and coarse mode) were found to fit well the in-situ measured size distributions during the campaign (Conant et al.

2003), only two modes were used here. The nucleation mode was disregarded, as it is not optically efficient in the sunphotometer wavelength range. The parameters of a bimodal lognormal size distribution were found by fitting the calculated to measured $\tau(\lambda_i)/\tau(0.525\ \mu\text{m})$, where $\lambda_i (i = 1, \ldots, 13)$ are the sunphotometer wavelengths. Using this normalization, the number of parameters to be retrieved was reduced, since the relative concentration of the two modes was retrieved instead of their individual concentrations. Since the mode radius and width of a lognormal size distribution retrieved from the optical depth spectrum are interdependent (a larger width of the distribution produces smaller values of mode radius, and vice versa) (Yu et al. 2000; Cachorro et al. 2000), the solutions in the present work were constrained by the widths of the in-situ measured size distributions. The values of these parameters for each layer studied here were found by fitting bimodal lognormal functions to the layer-averaged measured size distributions. Refractive index was used as an input parameter, together with the widths of the two size distribution modes. In the next step, the total particle number concentration, which provides the best fit of calculated optical thickness spectrum to the measured spectrum, was found.

4. RESULTS

During the Twin Otter's 19 flights as a part of the ACE-Asia campaign, the aerosol layers were sampled in horizontal legs, as well as in vertical profiles. As noted previously, the focus of this work was on layers observed in the same vertical profiles investigated in the radiative closure study by Wang et al. (2002). These are four Twin Otter vertical profiles in which two or three distinct layers were observed. Depending on particle composition, they classified the layers as boundary, pollution, and free tropospheric layers.

The optical thicknesses of the studied layers were calculated by subtracting optical depths measured at the bottom and the top of the layer. The uncertainties due to atmospheric horizontal inhomogeneity were estimated using the approach described by Redemann et al. (2003). Aerosol layer optical thicknesses were inverted to obtain size distributions, using both the CLI and NLS methods. The same constant refractive index value of 1.50–0.001i was used in all retrievals. The effect of unknown refractive index used in the retrieval will be discussed later.

Three free tropospheric layers were affected by dust particles (Wang et al. 2002). As noted by Sokolik et al. (2001) and Kalashnikova and Sokolik (2002, 2004), nonsphericity of dust particles should be accounted for in calculations of their optical properties, in order to obtain reliable results. Since both retrieval methods used here are based on Mie theory, the accuracy of the results of size distribution retrievals in the dust layers depends on the extent to which the modeled optical thicknesses are affected by particle nonsphericity. A study by Mishchenko et al. (1997), based on a model of a mixture of randomly oriented surface-equivalent prolate and oblate spheroids of different shapes, showed that the effect of particle nonsphericity on extinction is not significant. Assuming more representative dust particle shape models based on large number of dust particles collected in the atmosphere, Kalashnikova and Sokolik (2002, 2004) showed that a spherical model can significantly underpredict aerosol extinction (by ~33% at 0.55 μm in some cases). As they considered volume-equivalent spherical and nonspherical particles, a large difference in extinction coefficients is a consequence of larger surface area of nonspherical particles. They obtained various spherical/nonspherical aerosol extinction differences for a range of realistic nonspherical models. This suggests that an estimate of the effect of particle nonsphericity on the retrieved size distribution would require information on particle shape (which could be obtained by individual particle analysis). This effect is not investigated here. However, it is noteworthy that the retrieved size distributions (using an assumption of spherical particles) can be used for calculating aerosol optical properties important for estimating their radiative effects (single scattering albedo and asymmetry parameter). Mishchenko et al. (1997) showed that a model of surface-equivalent spherical particles could accurately estimate these aerosol properties.

4.1. Results of the Two Retrieval Methods

The major difference between the two retrieval methods used in this work is that the constrained linear inversion (CLI) method does not impose any constraints on the analytical form of the distribution to be retrieved, whereas the nonlinear least squares (NLS) method was used to derive parameters of a bimodal lognormal size distribution (with modal widths fixed by in-situ measurements). Comparison of results of the two retrieval methods, carried out for all the layers studied here, showed that there is a radius range (with the lower limit at ~0.1 μm, and the upper limit between ~1.2 μm and 2 μm) in which a fairly good agreement between the results of the two retrieval methods was achieved. Figure 1 shows that this is approximately the radius range in

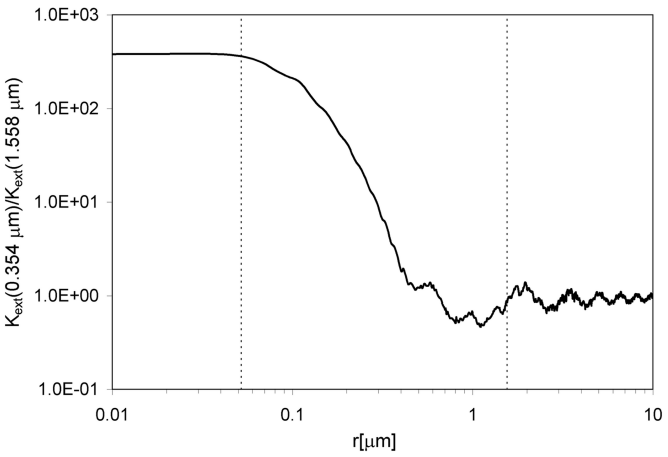

FIG. 1. Dependence of the ratio of extinction efficiencies at the smallest and the largest wavelengths of the AATS-14 measurements on particle size. Vertical dotted lines indicate the radius range of retrievable particle size distributions, according to the ratio criterion by Heintzenberg et al. (1981).

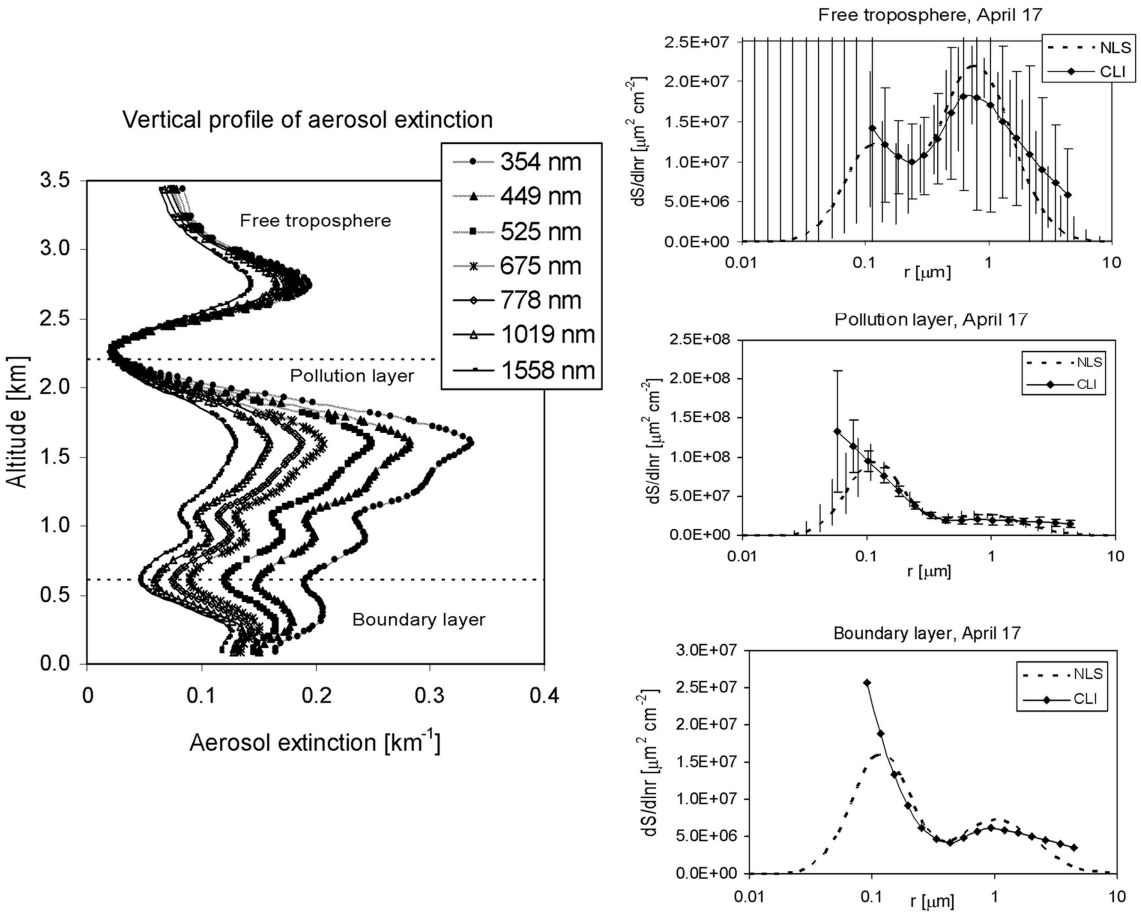

FIG. 2. (**left panel**) Vertical profile of aerosol extinction at different wavelengths, derived from sunphotometer measurements for April 17 (adapted from Schmid et al. 2003). (**right panel**) Retrieved aerosol size distributions in three layers in the vertical profile of April 17—comparison of two retrieval methods: non-linear least squares (NLS) and constrained linear inversion (CLI).

which, according to Heintzenberg et al.'s (1981) ratio criterion, meaningful solutions can be obtained from the measured optical thickness spectra. This criterion suggests that optical thickness spectra carry retrievable information on particle size distribution in the range of particle radii in which the ratio of kernel functions (or extinction efficiencies in this case) at the smallest and the largest wavelengths of the measurements varies with particle size. Outside this radius interval the differences between the two retrieval methods become large. In layers with significant fine particle mode, CLI method overestimates the particle concentration at radii smaller than ~ 0.1 μm, as a result of the assumption (used in the retrieval algorithm) that the particle concentration is zero beyond the radius range of retrievals.

As an example, comparisons for the layers observed in the April 17 profile are presented in Figure 2. The error bars in the retrieved size distributions are due to optical thickness uncertainties. They are omitted in the case of the boundary layer of the April 17 profile, since they are larger than the retrieved particle concentrations at all particle sizes in the range of retrieval, due to large uncertainties in the measured optical thickness. In all studied layers, the estimated size distribution uncertainties are large outside the radius range of retrievable size distributions, given in Figure 1. However, as pointed out by Russell et al. (1999), these errors do not represent all possible size distribution results.

Refractive index generally varies with particle radius due to the different chemical composition of particles of different sizes; this affects aerosol extinction spectra (Gillespie et al. 1978), and consequently the retrieved aerosol size distribution. While the CLI code used here was set up to perform retrievals under the assumption of a constant refractive index, the NLS algorithm can perform retrievals for a size-resolved refractive index. We therefore used the NLS retrieval method to carry out comparison between the size distributions retrieved using a size-resolved, and different constant values of refractive index.

The size-resolved refractive indices calculated by Wang et al. (2002) for the three distinct layers of the April 17 vertical profile were used. In the boundary layer, the refractive index did not show significant variability with particle size; the refractive index was real, and its value varied from 1.53–1.54 in the radius range 0.01–4.5 μm. As shown in the top panels of Figures 3

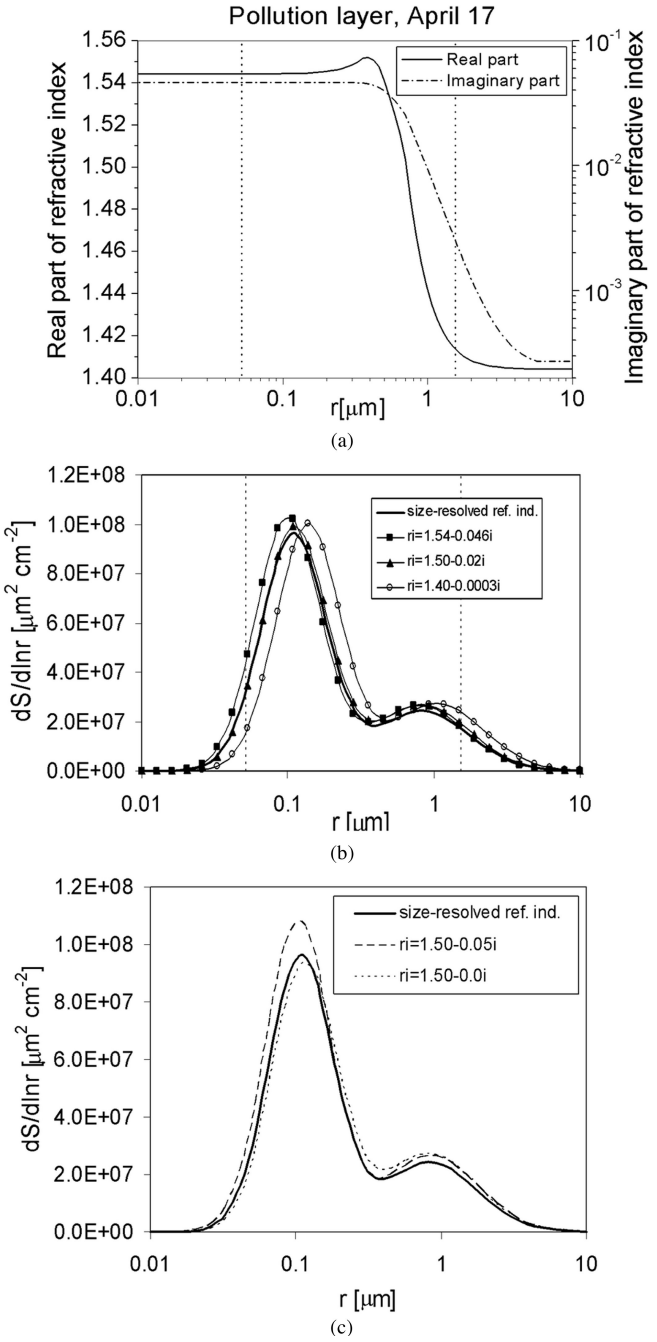

FIG. 3. (**a**) Dependence of aerosol refractive index on particle size, for the pollution layer of the April 17 profile. Vertical dotted lines show the radius range of retrievable size distributions (see Figure 1); (**b**) Size distributions retrieved using the NLS method, for size-resolved refractive index shown in (a), and constant refractive index values selected from the range given in (a). (**c**) Comparison of the size distributions retrieved using size-resolved refractive index, and two constant refractive indices with different imaginary parts.

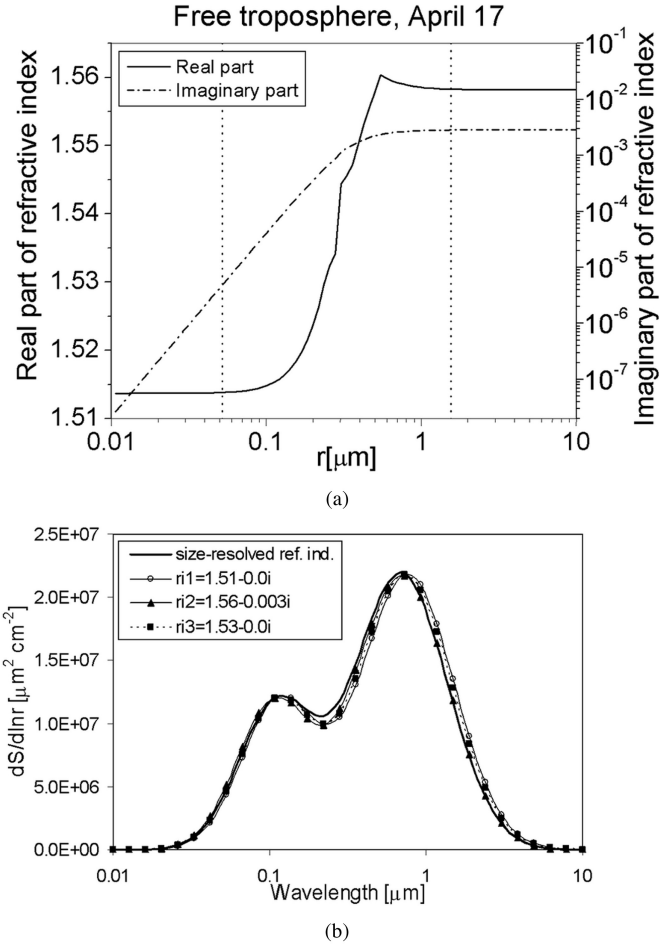

FIG. 4. (**a**) Dependence of aerosol refractive index on size, for the free tropospheric layer of the April 17 profile. Vertical dotted lines show the radius range of retrievable size distributions (see Figure 1); (**b**) Size distributions retrieved using the NLS method, for size-resolved refractive index shown in (a), and constant refractive index values selected from the range given in (a).

and 4, the variability was significantly larger in the pollution and free tropospheric layers. The presence of elemental carbon and dust in the pollution layer, and dust in the free tropospheric layer (Wang et al. 2002), led to a non-zero imaginary part of the refractive index in these layers.

Figures 3 and 4 show comparisons of size distributions obtained using a size-resolved refractive index calculated by Wang et al. (2002), and different constant refractive indices selected from a range of values at different radii. As seen from these results, an assumption of a constant refractive index causes a shift of the size distribution, compared to the result of retrieval in which a size-resolved refractive index was used, while the shape of the distribution (determined by the relative contribution of fine and coarse particle modes) is maintained. If a constant refractive index of the particles that contribute significantly to extinction in the given wavelength range is assumed in the retrieval, the resulting size distribution is in agreement with the one obtained from an assumption of a size-dependent refractive index. This is more clearly seen in the case of the pollution layer, due to larger variability of the refractive index with particle size. The largest shift of the retrieved size distribution occurs when the refractive index of large particles, outside the range of retrievable size distribution, is used. However, the size distribution retrieved assuming the refractive index value of 1.50–0.02i (within the

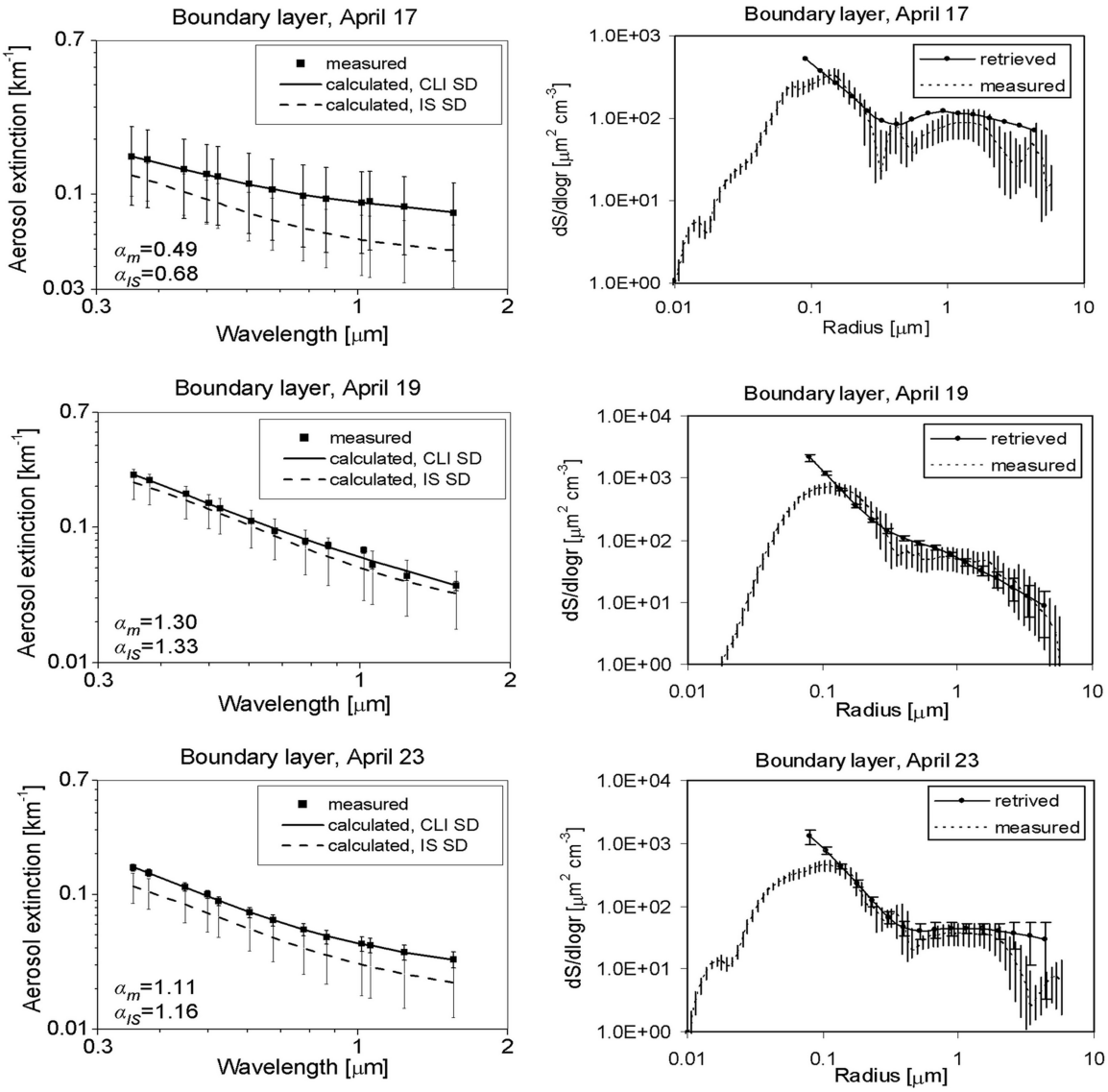

FIG. 5. Boundary layers: (**left panels**) Layer optical thickness spectra (measured, calculated from retrieved size distribution (CLI) and calculated from in-situ measured size distribution averaged over the layer (IS)); α_m and α_{IS} are the Ångström exponents for the measured optical thickness spectra, and those calculated from the in-situ measured size distributions, respectively; (**right panels**) Retrieved and measured size distributions.

range of retrievable size distributions) is in agreement with that retrieved using the size-resolved refractive index. As seen in the bottom panel of Figure 3, an unknown imaginary part of the refractive index mainly affects the particle concentration, in agreement with results by King et al. (1978) and Gonzalez Jorge and Ogren (1996).

4.2. Comparison of Retrieved and In-Situ Measured Size Distributions

Since the distributions obtained as a result of the NLS algorithm were required to have the same modal widths as those measured in-situ, the NLS and in-situ results are not independent. Therefore, comparison of the NLS results with the measured size distributions was not studied. Comparisons of the size distributions retrieved using the constrained linear inversion method with those measured in-situ are presented in Figures 5–7. All size distributions were retrieved using the same constant refractive index $m = 1.50–0.001i$. King et al. (1978) and Gonzalez Jorge and Ogren (1996) noted that the uncertainties in retrieval using the CLI method due to unknown refractive index were not critical. They found that a wrong assumption of the refractive index value results in a small shift of the size distribution, whereas the distribution shape is not changed.

For the purpose of comparison, the in-situ measured size distributions were averaged within each of the studied layers. The retrieved size distributions are representative of a layer vertical column, whereas those measured in-situ represent distributions at a given altitude. Therefore, the retrieved size distributions

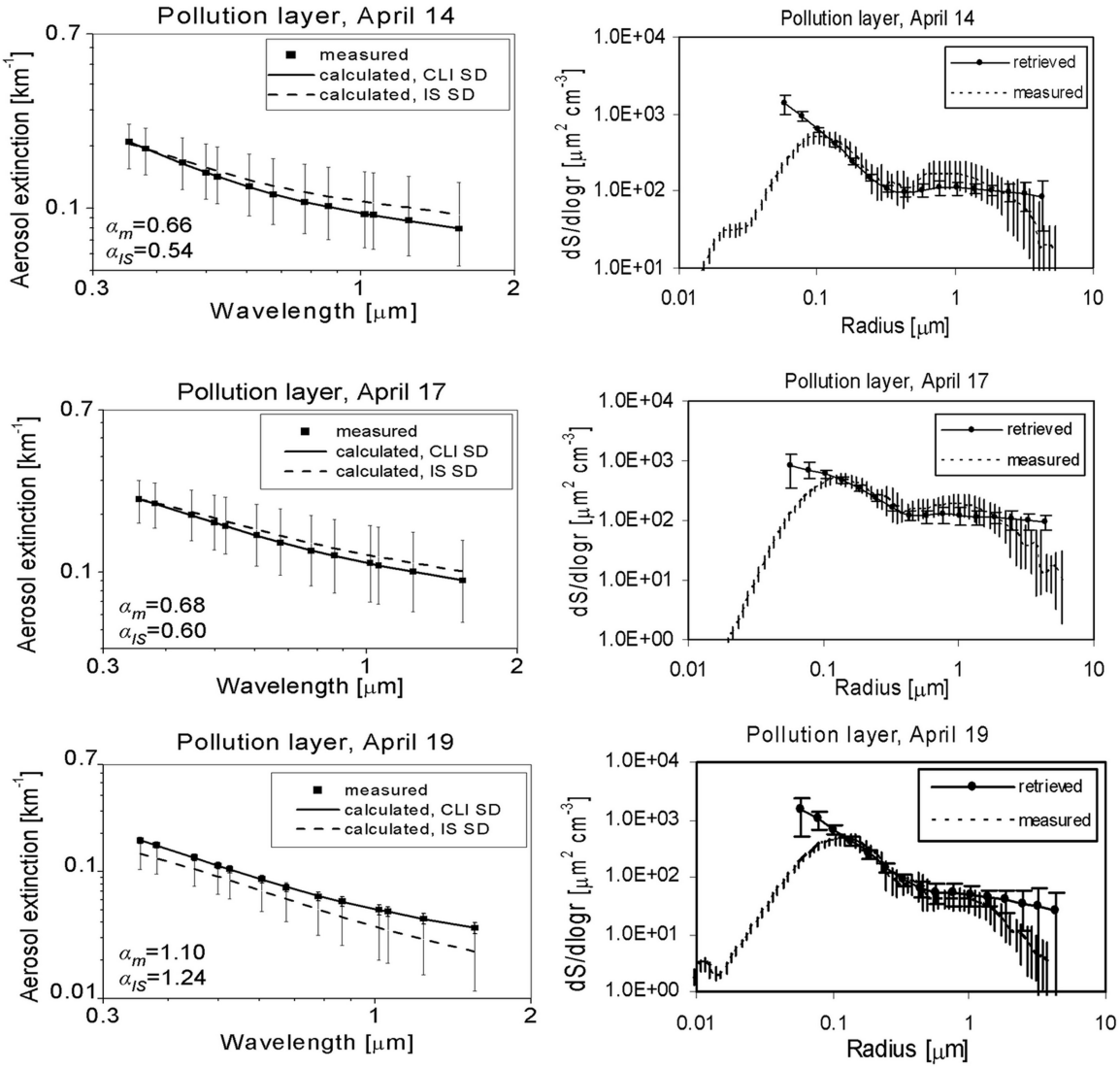

FIG. 6. Same as Figure 5, except for pollution layers.

were renormalized for these comparisons by dividing total number concentration by the layer thickness. Figures 5–7 also show the corresponding extinction spectra. The average extinctions that follow from the in-situ measured size distributions in the same layers were calculated previously by Wang et al. (2002), for comparison with the sunphotometer measurements. They used a size-resolved refractive index for this purpose. For better understanding of the size distribution comparisons, these calculations were repeated in the present work, using the same constant refractive index that was used for the size distribution retrievals. The error bars in these extinction coefficients are due to uncertainties in the measured size distributions. To translate the measured layer optical thickness of each layer into extinction, it was also divided by the layer geometrical thickness.

Both the retrieved and in-situ measured size distributions in the boundary and pollution layers (Figures 5 and 6) exhibited a dominant fine particle mode (particle radii smaller than $\sim$0.4 μm). However, the contribution of large particles to the optical thickness spectra is considerable in all layers studied here, as indicated by Ångström exponent (defined below) values given in Figures 5–7, for the sunphotometer-measured optical thickness spectra and those calculated from the in-situ measured size distributions. Comparison of retrieved and in-situ measured size distributions in these layers show that, while there are discrepancies consistent with disagreements between the corresponding extinction spectra, the shape of the size distribution is well reproduced in most cases. The size distributions in Figures 5–7 are presented on a log-log scale, in order to show coarse mode particle surface concentration more clearly.

We use the Ångström exponent α (Ångström 1929) to describe the wavelength dependence of aerosol optical thickness.

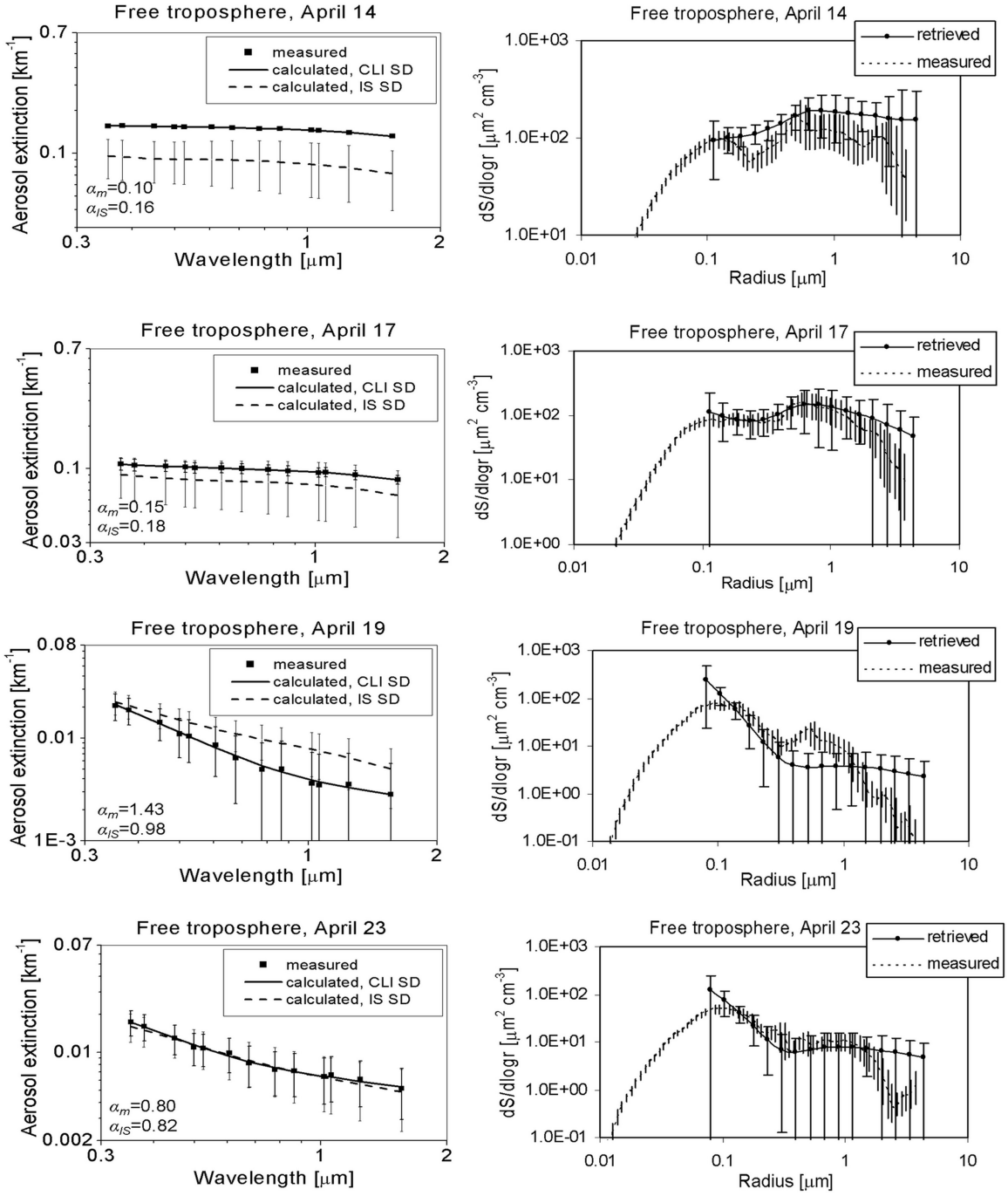

FIG. 7. Same as Figure 5, except for free tropospheric layers.

It is obtained from a linear least-squares fit of optical thickness spectra to the formula:

$$\ln \tau(\lambda) = -\alpha \ln \lambda + \beta, \qquad [11]$$

where β is the turbidity coefficient. While a second order polynomial describes more accurately the $\ln \tau$ versus $\ln \lambda$ relationship (King and Byrne 1976; Eck et al. 1999; Schmid et al. 2003), most discrepancies between the measured and retrieved size distributions in this work can be explained by comparison of the Ångström exponent values for the corresponding optical thickness spectra.

We carried out a sensitivity analysis to examine to what degree the CLI method can be expected to resolve the aerosol size distribution. For that purpose, bimodal lognormal aerosol size distributions, with the parameters given in Table 1, were used to generate aerosol optical thickness spectra in the

TABLE 1
Parameters of bimodal lognormal aerosol size distributions used to generate optical thickness spectra for sensitivity analysis

Size distributions	SD1	SD2	SD3	SD4	SD5	SD6	SD7	SD8	SD9	SD10
Modal radius [μm]	0.08	0.08	0.08	0.08	0.08	0.08	0.08	0.08	0.08	0.08
	0.60	1.00	0.60	1.00	0.60	1.00	0.60	1.00	1.00	2.50
Width	0.40	0.40	0.60	0.60	0.40	0.40	0.60	0.60	0.40	0.40
	0.60	0.80	0.60	0.80	0.60	0.80	0.60	0.80	0.80	0.80
α	0.5	0.5	0.5	0.5	1.1	1.1	1.1	1.1	0.1	0.1

AATS-14 wavelength range. The concentrations of the two modes were adjusted to yield an aerosol optical thickness $\tau(0.5\ \mu\text{m}) = 1$, with wavelength dependencies given by Ångström exponent values (α) of ~ 0.5 and 1.1, in the AATS-14 wavelength range. The cases of dominant coarse mode ($\alpha \sim 0.1$) will be discussed later in this section. We used four different size distributions to generate similar optical thickness spectra (similar Ångström exponents). Inversion of these optical thickness spectra resulted in size distributions which exhibited generally good agreement with the original size distributions in the $\sim$0.08–2 μm, as shown in Figure 8. The size distribution retrievals were more successful in cases with a larger contribution of the coarse mode to the wavelength dependence of optical thickness ($\alpha \sim 0.5$), particularly for the cases with the coarse mode at smaller radii. In the cases with dominant fine mode ($\alpha \sim 1.1$), the coarse mode was not well resolved: the retrieved surface area in this mode was smaller than that in the original size distribution, while the minimum between the two modes was higher. Gonzalez Jorge and Ogren (1996) reported a similar result and explained it by the retrieval algorithm retrieving the fine mode first, while the coarse mode is included to get closer agreement between measured and calculated extinction spectra. The optical thickness spectra with $\alpha \sim 0.5$ which correspond to size distributions with considerably different shapes as a result of differences in the coarse mode (top two panels in Figure 8) exhibit relative differences larger than the uncertainties in measured optical thicknesses with similar wavelength dependencies (pollution layers of April 14 and April 17). In cases of larger Ångström exponent ($\alpha \sim 1.1$), the relative differences are smaller, due to smaller contribution of large particles to optical thickness.

Inversion of generated optical thickness spectra performed using the NLS retrieval method resulted in size distributions in excellent agreement with the original distributions. Variation of the widths of the size distribution lognormal modes (used as an input in the retrieval algorithm) by ± 0.5 caused small variations in resulting particle surface area in the radius range between $\sim$0.1 and 1.6 μm. The variations were significant outside this range.

An example of the agreement between the shapes of the retrieved and measured size distributions is the case of the boundary layer of April 23 (Figure 5). Larger differences at the ends of the radius interval of the retrieval are not reflected in the wavelength dependence of the extinction. Discrepancies between the corresponding extinctions could be the result of lower resolution of the size distribution measurements. Differences between the retrieved and measured size distributions that appear in the boundary layer of April 17, are in accord with the differences in extinction spectra derived from the in-situ measurements and those measured using the sunphotometer. Wang et al. (2002) explained these differences in extinction spectra by horizontal inhomogeneity of the observed layer, which affected the sunphotometer measurements, and supported this assumption by comparison of extinctions derived from the measured size distributions with the lidar-derived extinction. Significant discrepancies between the retrieved and measured size distributions in the free tropospheric layer of the April 14 profile can also be explained by layer horizontal inhomogeneity (Wang et al. 2002).

Two free tropospheric layers (April 14 and April 17) studied here were reported to contain a significant amount of dust in the coarse particle mode (Wang et al. 2002). The retrieved and measured size distributions exhibit differences in these layers, and the corresponding extinction spectra deviate from each other. Wang et al. (2002) indicated that counting statistics of the size distribution measurements and accuracy of interpretation of the Aerodynamic Particle Sizer measurements (due to particle nonsphericity) were some of the possible causes of these discrepancies. Huebert et al. (2003) reported that APS undersized or undercounted particles in the dust layers during the ACE-Asia campaign, probably due to particle nonsphericity. Additionally, nonsphericity of dust particles was not taken into account in size distribution retrievals in this work, as noted earlier. Layer horizontal inhomogeneity, mentioned above, is probably responsible for larger discrepancies in the dust layer of April 14. It should be noted that particles larger than the size range of APS measurements could also explain the difference between the optical thicknesses obtained from sunphotometer measurements and calculated from measured size distribution in two dust layers. An increase in the concentration of large particles leads to an increase in optical thickness, not affecting its wavelength dependence. However, in the case of size distributions in which the coarse mode is not a dominant contributor to optical thickness in the AATS-14 wavelength range (Ångström exponent larger than $\sim$0.5), an increase in the amount of aerosol in the $r_p > 1.5\ \mu$m size range (r_p is particle radius) results not only in an increase in optical thickness, but also a change in its wavelength

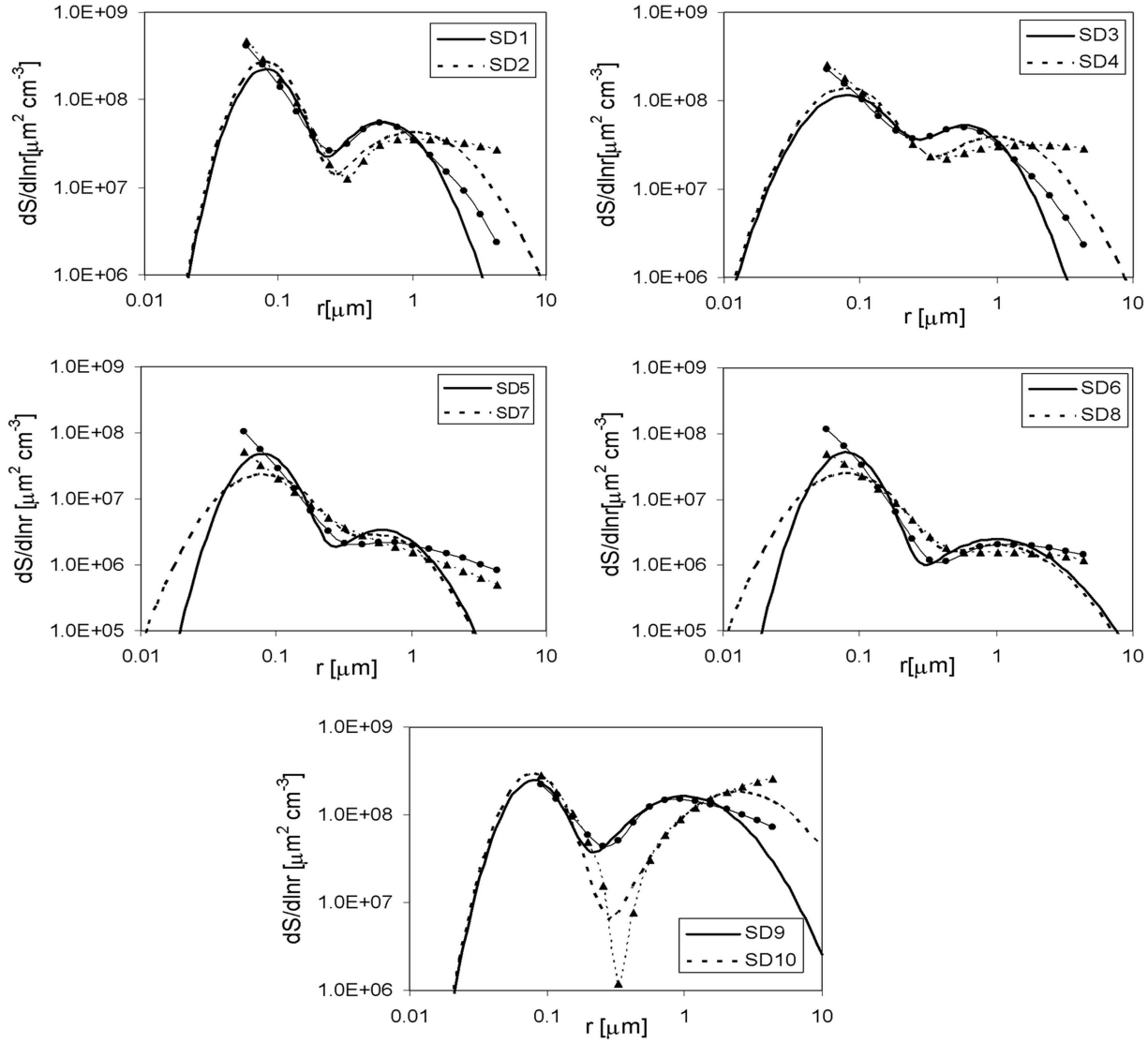

FIG. 8. Aerosol size distributions used to generate optical thickness spectra for sensitivity analysis (lines) and corresponding retrieved size distributions (lines with symbols).

dependence. We also performed size distribution retrievals from generated optical thickness spectra with weak wavelength dependence (α between 0.1 and 0.2). In these cases, in which the contribution of the coarse mode to optical thickness spectra was dominant, the coarse mode was retrieved better if radii below $\sim$0.1 were not included in the radius range of retrieval. The fine mode was, however, not reproduced successfully.

In addition to those size distributions in agreement with the DMA/APS measurements, it was of interest to consider distributions with their coarse mode at larger radii for generating optical thickness spectra with weak wavelength dependencies for our sensitivity analysis. The presence of larger particles in the dust layers during ACE-Asia is supported by results presented by Moore et al. (2004). They reported surface area size distributions with coarse mode centered at 2.5 μm particle radius, and significant particle concentration at 5 μm, obtained from measurements using airborne Forward Scattering Spectrometer Probes (FSSP) as a part of ACE-Asia and TRACE-P campaigns. FSSPs were mounted on aircraft wings and were not affected by inlet losses: they measured size distributions under ambient conditions. The bottom panel in Figure 8 shows an example of results of the sensitivity analysis performed for the cases in which the coarse mode is the dominant contributor to the aerosol optical thickness ($\alpha \sim 0.1$). The two size distributions presented differ in the position of the coarse mode (the modal radii are 1.0 and 2.5 μm), while the remaining size distribution parameters (given in Table 1) are the same. Both size distributions are scaled to yield τ (0.5 μm) = 1.0. The relative contribution of the coarse mode to the total aerosol optical thickness in the two cases is similar: 70–100% in the AATS-14 wavelength range. The coarse

TABLE 2

Effective radii (in μm) for the retrieved size distributions (using both the CLI and NLS methods) and those measured in-situ. Percentages given in parentheses are the relative differences between the in-situ derived and the retrieved values

	April 12		April 17			April 19			April 23	
	PL	FT	BL	PL	FT	BL	PL	FT	BL	FT
CLI	0.402 (−16%)	1.354 (71%)	0.418 (−19%)	0.481 (−4%)	1.029 (57%)	0.192 (−16%)	0.220 (3%)	0.198 (−0.4%)	0.291 (33%)	0.393 (53%)
NLS	0.361 (−25%)	1.259 (59%)	0.576 (11%)	0.415 (−17%)	0.722 (10%)	0.138 (−40%)	0.201 (−6%)	0.133 (−33%)	0.155 (−29%)	0.209 (−18%)
In-situ	0.481	0.792	0.519	0.498	0.656	0.229	0.213	0.199	0.219	0.256

modes of both size distributions are retrieved more successfully if particles of sizes below 0.08 μm are not included in the radius range of retrieval. The particles with $r_p > 1.5$ μm contribute significantly to aerosol optical thickness in the two cases presented: approximately 20–30% in the case of coarse mode at 1 μm, and 50–70% in the case of coarse mode at 2.5 μm. As discussed earlier, according to the criterion by Heintzenberg et al. (1981), aerosol optical thickness spectra measured using AATS-14 contain retrievable information on particle size distribution in the 0.05–1.5 μm radius range (Figure 1): at $r_p > 1.5$ μm, particles of certain size can be replaced by a number of particles of different size without noticeably affecting the optical thickness spectrum. As a result, the coarse mode of the size distribution is not well resolved. The retrieval of the coarse mode is, however, more successful in the case in which this mode is centered at a radius within the size range of retrievable size distribution. The overestimation of particle surface area at the large end of the radius range of retrieval is less significant in this case. Furthermore, the contribution of the particles beyond the radius range of retrieval in this paper ($r_p > 5$ μm) is not insignificant in the case of a coarse mode radius of 2.5 μm: 11–14% for the case shown in Figure 8. The extension of the radius range of retrieval to larger particle sizes results in an unstable solution because of the larger size interval with no retrievable information on aerosol size distribution.

4.3. Effective Radius

Due to similar shapes of retrieved and in-situ measured size distributions, it was of interest to compare the corresponding effective radii. Effective radius is of interest in studies of aerosol radiative forcing (Tegen and Lacis 1996), and is defined as:

$$r_{eff} = \frac{M_3}{M_2} = \frac{3V}{S}, \qquad [12]$$

where S and V are total particle surface area and volume concentration, and M_k is a k*th* moment of the size distribution, defined as:

$$M_k = \int_0^\infty r^k n(r)\, dr. \qquad [13]$$

In the case of a lognormal size distribution, the moments become (Lenoble and Brogniez 1984):

$$M_k = r_m^k \exp\left(\frac{1}{2}k^2\sigma^2\right), \qquad [14]$$

which leads to the following formula for effective radius:

$$r_{eff} = r_m \exp\left(\frac{5}{2}\sigma^2\right). \qquad [15]$$

The effective radii calculated from retrieved and measured aerosol size distributions for all the layers studied here are given in Table 2. The results show that the two retrieval methods yield generally different particle effective radii. However, these differences mainly occurred due to differences in size distributions at radii where no retrievable information on size distribution is contained in the optical thickness measurements.

In the boundary and pollution layers, effective radii obtained from the CLI retrieval method are generally in agreement with those obtained from in-situ measured size distributions within the same layers, in accord with close size distribution shapes in most cases. Overestimated total surface area and volume resulting from this retrieval method (mainly due to large concentrations at the ends of the retrieved size distributions) cancel out to a large extent when calculating the effective radius. In the dust layers, however, the CLI method overestimates effective radius: this is due to its inability to resolve the fine particle mode, since this mode is not a dominant contributor to the wavelength dependence of the measured optical thickness (as suggested by their small Ångström exponent). Note that in the case of the free tropospheric layers of April 19 and April 23, comparison between the effective radii obtained from CLI-retrieved and measured size distributions is not consistent with the comparison of the corresponding Ångström exponent values. These layers are optically thin, which resulted in significant uncertainties in retrieved size distributions.

Discrepancies between the effective radii derived from retrieved and measured size distributions in some cases are partly due to unknown refractive index. Although uncertainty in the refractive index does not have a significant effect on the shape of the retrieved size distribution, it affects the integrated properties, and therefore the effective radius. Gonzalez Jorge and Ogren (1996) reported an average error of 2–9% in the effective radius, as a result of uncertainty in refractive index, assuming that the true particle refractive index is constant. According to their results, this error becomes larger if the true particle refractive index varies with size.

5. CONCLUSION

Aerosol size distributions were retrieved from layer optical thickness spectra, measured in the wavelength range 0.354–1.558 μm, using the airborne NASA AATS-14 sunphotometer, during the ACE-Asia campaign. Two retrieval methods employed for this purpose used different assumptions: the constrained linear inversion method used a second derivative smoothness constraint and no assumption about the shape of the size distribution to be retrieved; the non-linear least squares algorithm was shape-constrained and was used for retrieval of parameters of a bimodal lognormal size distribution. Intercomparison of the two retrieval methods, carried out for distinct layers observed in four vertical profiles, showed agreement in the radius interval from ~0.1 μm to ~(1.2–2 μm), which was found to be close to the resolvable radius range in the wavelength range of the optical thickness measurements.

However, discrepancies were large outside this interval, due to lack of information on particles of these radii in the measured optical thickness. Consequently, the effective radii resulting from the two retrieval methods exhibited differences in most cases.

Retrieved aerosol size distributions were compared with the corresponding in-situ measured distributions averaged within each of the studied layers. The shapes of the retrieved size distributions were generally in agreement with those measured in-situ, in the boundary and pollution layers, dominated by small particles. This is consistent with the close wavelength dependencies of the corresponding extinctions. Consequently, the corresponding effective radii showed fairly good agreement. However, the agreement was not achieved in the dust layers, partly due to the inability of the constrained linear inversion method to resolve the fine particle mode in these layers. In addition, particle nonsphericity was not accounted for in the retrieval, and it is not clear what effect it would have on the results. Moreover, Wang et al. (2002) noted that in-situ measured size distributions were affected by particle nonsphericity, since interpretation of APS measurements depends on particle shape. The large discrepancy between the optical thicknesses derived from the sunphotometer measurements and from the measured size distribution in two dust layers studied can be explained by particles larger than the size range of APS measurements.

Comparison of size distributions retrieved using a size-resolved refractive index (based on particle chemical composition), and different constant refractive index values, was carried out for two layers. These comparisons show that a constant refractive index, pertaining to particle sizes within the interval of retrievable size distributions, yields a size distribution which is in agreement with the one retrieved using a size-resolved refractive index.

REFERENCES

Ångström, A. (1929). On the Atmospheric Transmission of Sun Radiation and on Dust in the Air, *Geogr. Ann*. 11:156–166.

Bane, J. M., Bluth, R., Flagg, C., Jonsson, H., Melville, W. K., Prince, M., and Riemer, D. (2004). UNOLS now Overseas Research Aircraft Facilities for Ocean Science, *Eos. Trans. AGU* 85(41):402.

Ben-David, A., Herman, B. M., and Reagan, J. A. (1988). Inverse Problem and the Pseudoempirical Orthogonal Function Method of Solution. 2: Use, *Appl. Optics*. 27:1243–1254.

Bluth, R. T., Durkee, P. A., Seinfeld, J. H., Flagan, R. C., Russell, L. M., Crowley, P. A. and Finn, P. (1996). Center for Interdisciplinary Remotely-Piloted Aircraft Studies (CIRPAS), *Bull. Amer. Meteor. Soc*. 77:2691–2699.

Box, G. P., Sealey, K. M., and Box, M. A. (1992). Inversion of Mie Extinction Measurements Using Analytic Eigenfunction Theory, *J. Atmos. Sci*. 49:2074–2081.

Brogniez, C., and Lenoble, J. (1988). Size Distribution of Stratospheric Aerosols from SAGE II Multiwavelength Extinctions. In P. V. Hobbs and M. P. McCormick (eds.), *Aerosols and Climate*. A. Deepak, Hampton, VA, 305–311.

Cachorro, V., Duran, P., Vergaz, R., and de Frutos, A. M. (2000). Columnar Physical and Radiative Properties of Atmospheric Aerosols in North Central Spain, *J. Geophys. Res*. 105 (D6):7161–7175.

Conant, W. C., Seinfeld, J. H., Wang, J., Carmichael, G. R., Tang, Y., Uno, I., Flatau, P. J., Markowicz, K. M., and Quinn, P. K. (2003). A model for the Radiative Forcing During ACE-Asia Derived from CIRPAS Twin Otter and R/V *Ronald H Brown* Data and Comparison with Observations, *J. Geophys. Res*. 108 (D23), 8661, doi:10.1029/2002JD003260.

D'Almeida, G. A., Koepke, P., and Shettle, E. P. (1991). *Atmospheric Aerosols: Global Climatology and Radiative Characteristics*. A. Deepak, Hampton, VA.

De Rooij W. A., and Van Der Stap, C. C. A. H. (1984). Expansion of Mie Scattering Matrices in Generalized Spherical Functions, *Astronomy and Astrophysics*. 131:237–248.

Dubovik, O. V., Lapyonok, T. V., and Oshchepkov, S. L. (1995). Improved Technique for Data Inversion: Optical Sizing of Multicomponent Aerosols, *Appl. Optics*. 34:8422–8437.

Eck, T. F., Holben, B. N., Reid, J. S., Dubovik, O., Smirnov, A., O'Neill, N. T., Slutsker, I., and Kinne, S. (1999). Wavelength Dependence of the Optical Depth of Biomass Burning, Urban, and Desert Dust Aerosols, *J. Geophys. Res*. 104 (D24):31,333–31,349.

Gillespie, J. B., Jennings, S. G., and Lindberg, J. D. (1978). Use of an Average Refractive Index in Atmospheric Propagation Calculations, *Appl. Opt*. 17:989–991.

Gonzalez Jorge, H. and Ogren, J. A. (1996). Sensitivity of Retrieved Aerosol Properties to Assumptions in the Inversion of Spectral Optical Depths, *J. Atmos. Sci*. 53:3669–3683.

Hegg, D., Covert, D. S., Jonsson, H., and Covert, P. A. (2005). Determination of the Transmission Efficiency of an Aircraft Aerosol Inlet, *Aerosol Sci. Technol*. 39:966–971.

Heintzenberg, J., Muller, H., Quenzel, H., and Thomalla, E. (1981). Information Content of Optical Data with Respect to Aerosol Properties: Numerical Studies with a Randomized Minimization-Search-Technique Inversion Algorithm, *Appl. Opt*. 20:1308–1315.

Huebert, B. J., Bates, T., Russell, P. B., Shi, G., Kim, Y. J., Kawamura, K., Carmichael, G., and Nakajima, T. (2003). An Overview of ACE-Asia: Strategies for Quantifying the Relationships between Asian Aerosols and their Climate Impacts, *J. Geophys. Res*. 108 (D23), 8633, doi:10.1029/2003JD003550.

Junge, C. E. (1955). The Size Distribution and Aging of Natural Aerosols as Determined from Electrical and Optical Data in the Atmosphere, *J. Meteor.* 12:13–25.

Kalashnikova, O., and Sokolik, I. N. (2002). Importance of Shapes and Composition of Wind-Blown Dust Particles for Remote Sensing at Solar Wavelengths, *Geophys. Res. Lett*. 29, No. 10, 10.1029/2002GL014947.

Kalashnikova, O. V., and Sokolik, I. N. (2004). Modeling the Radiative Properties of Nonspherical Soil-Derived Mineral Aerosols, *JQSRT* 87:137–166.

King, M. D., and Byrne, D. M. (1976). A Method for Inferring Total Ozone Content from Spectral Variation of Total Optical Depth Obtained with a Solar Radiometer, *J. Atmos. Sci.* 33:2242–2251.

King, M. D., Byrne, D. M., Herman, B. M., and Reagan, J. A. (1978). Aerosol Size Distributions Obtained by Inversion of Spectral Optical Depth Measurements, *J. Atmos. Sci*. 35:2153–2167.

King, M. D. (1982). Sensitivity of Constrained Linear Inversions to the Selection of the Lagarange Multiplier, *J. Atmos. Sci*. 39:1356–1369.

Kuzmanoski M., Box, M. A., Schmid, B., Box, G. P., Wang, J., Russell, P. B., Bates, D., Jonsson, H. H., Welton, E. J., and Seinfeld, J. H. (2006). Aerosol Properties Computed from Aircraft-Based Observations During the ACE-Asia Campaign: 2. A Case Study of Lidar Ratio Closure, *Aerosol Science and Technology* (in press).

Lenoble, J., and Brogniez, C. (1984). A Comparative Review of Radiation Aerosol Models, *Beitr. Phys. Atmos*. 57:1–20.

McMurry, P. H. (2000). A review of Atmospheric Aerosol Measurements, *Atmos. Environ*. 34:1959–1999.

Mishchenko, M. I., Dlugach, J. M., Yanovitskij, E. G., and Zakharova, N. T. (1999). Bidirectional Reflectance of Flat, Optically Thick Particulate Layers: an Efficient Radiative Transfer Solution and Applications to Snow and Soil Surfaces, *J. Quant. Spectrosc. Radiat. Transfer.* 63:409–432.

Mishchenko, M. I., Travis, L. D., Kahn, R. A., and West, R. A. (1997). Modeling Phase Functions for Dustlike Tropospheric Aerosols Using a Shape Mixture

of Randomly Oriented Polydisperse Spheroids, *J. Geophys. Res.* 102:16,831–16,847.

More, J. J. (1977). The Levenberg-Marquardt Algorithm: Implementation and Theory, in *Numerical Analysis. Lect. Notes in Math.* vol. 630, G. A. Watson (Ed.), Springer-Verlag, New York.

Moore, K. G., Clarke, A. D., Kapustin, V. N., McNaughton, C., Anderson, B. E., Winstead, E. L., Weber, R., Ma, Y., Lee, Y. N., Talbot, R., Dibb, J., Anderson, T., Doherty, S., Covert, D., and Rogers, D. (2004). A Comparison of Similar Aerosol Measurements made on the NASA P3-B, DC-8, and NSF C-130 Aircraft during TRACE-P and ACE-Asia, *J. Geophys. Res.* 109 (D15), D15S15, doi:10.1029/2003JD003543.

Nakajima, T., Tonna, G., Rao, R., Boi, P., Kaufman, Y., and Holben, B. (1996). Use of Sky Brightness Measurements from Ground for Remote Sensing of Particulate Polydispersions, *Appl. Optics* 35:2672–2686.

Redemann, J., Masonis, S., Schmid, B., Anderson, T., Russell, P., Livingston, J., Dubovik, O., and Clarke, A. (2003). Clear-Column Closure Studies of Aerosols and Water Vapor Aboard the NCAR C-130 in ACE-Asia, 2001. *J. Geophys. Res.* 108 (D23), 8655, doi:10.1029/2003JD003442.

Reid, J. S., Hobbs, P. V., Ferek, R. J., Blake, D. R., Martins, J. V., Dunlap, M. R., and Liousse, C. (1998). Physical, Chemical, and Optical Properties of Regional Hazes Dominated by Smoke in Brazil, *J. Geophys. Res.* 103 (D24), 32,059–32,080.

Russell, P. B., Livingston, J. M., Hignett, P., Kinne, S., Wong, J., Chien, A., Bergstrom, R., Durkee, P., and Hobbs, P. V. (1999). Aerosol-Induced Radiative flux Changes off the United States Mid-Atlantic Coast: Comparison of Values Calculated from Sunphotometer and in situ Data with those Measured by Airborne Pyranometer, *J. Geophys. Res.* 104 (D2):2289–2307.

Schmid, B., et al. (2000). Clear-sky Closure Studies of Lower Tropospheric Aerosol and Water Vapor During ACE-2 Using Airborne Sunphotometer, Airborne in-situ, Apace-Borne, and Ground-based Measurements, *Tellus* 52B:568–593.

Schmid, B., Hegg, D. A., Wang, J., Bates, D., Redemann, J., Russell, P. B., Livingston, J. M., Jonsson, H. H., Welton, E. J., Seinfeld, J. H., Flagan, R. C., Covert, D. S., Dubovik, O., and Jefferson, A. (2003). Column Closure Studies of Lower Tropospheric Aerosol and Water Vapor During ACE-Asia Using Airborne Sun Photometer and Airborne in situ and Ship-based Lidar Measurements, *J. Geophys. Res.* 108 (D23), 8656, doi:10.1029/2002JD003361.

Sokolik I. N., Winker, D. M., Bergametti, G., Gillette, D. A., Carmichael, G., Kaufman, Y. J., Gomes, L., Schuetz, L., and Penner, J. E. (2001). Introduction to Special Section: Outstanding Problems in Quantifying the Radiative Impacts of Mineral Dust, *J. Geophys. Res.* 106 (D16): 18,015–18,027.

Svenningsson, I. B., Hansson, H.-C., Wiedensohler, A., Ogren, J. A., Noone, K. J., and Hallberg, A. (1992). Hygroscopic Growth of Aerosol Particles in the Po Valley, *Tellus* 44 B:556–569.

Tegen, I., and Lacis, A. A. (1996). Modeling of Particle Size Distribution and its Influence on the Radiative Properties of Mineral Dust Aerosol, *J. Geophys. Res.* 101 (D14):19,237–19,244.

Twomey, S. (1977). *Introduction to the Mathematics of Inversion in Remote Sensing and Indirect Measurements*. Elsevier, Oxford, UK, p. 342.

Wang, P.-H., McCormick, M. P., Swissler, T. J., Osborn, M. T., Fuller, W. H., and Yue, G. K. (1989). Inference of Stratospheric Aerosol Composition and Size Distribution from SAGE II Satellite Measurements, *J. Geophys. Res.* 94 (D6):8435–8446.

Wang, P.-H., Kent, G. S., McCormick, M. P., Thomason, L. W., and Yue, G. K. (1996). Retrieval Analysis of Aerosol Size Distribution Using Simulated Extinction Measurements at SAGE III Wavelengths, *Appl. Opt.* 35:433–440.

Wang, J., Flagan, R. C., Seinfeld, J. H., Jonsson, H. H., Collins, D. R., Russell, P. B., Schmid, B., Redemann, J., Livingston, J. M., Gao, S., Hegg, D. A., Welton, E. J., and Bates, D. (2002). Clear-Column Radiative Closure during ACE-Asia: Comparison of Multiwavelength Extinction Derived from Particle Size and Composition with Results from Sun Photometry, *J. Geophys. Res.* 107 (D23), 4688, doi:10.1029/2002JD002465.

Yu, S., Saxena, V. K., Wenny, B. N., DeLuisi, J. J., Yue, G. K., and Petropavlovskikh, I. V. (2000). A study of the Aerosol Radiative Properties needed to Compute Direct Aerosol Forcing in the Southeastern United States, *J. Geophys. Res.* 105 (D20):24,739–24,749.

Yue, G. K., McCormick, M. P., and Chu, W. P. (1986). Retrieval of Composition and Size Distribution of Stratospheric Aerosols with the SAGE II Satellite Experiment, *J. Atmos. Oceanic Technol.* 3:371–380.